Drastic reduction of the *R*-Fe exchange in interstitially modified (Nd, Ho)$_2$Fe$_{14}$B compounds probed by megagauss magnetic fields

N. V. Kostyuchenko,[1,*] I. S. Tereshina,[2] E. A. Tereshina-Chitrova,[3,4] L. A. Ivanov,[2] M. Paukov,[4,5] D. I. Gorbunov,[6] A. V. Andreev,[3] M. Doerr,[7] G. A. Politova,[8,9] A. K. Zvezdin,[10,11] S. V. Veselova,[2] A. P. Pyatakov,[2] A. Miyata,[12] O. Drachenko,[12] and O. Portugall[12]

[1]*Moscow Institute of Physics and Technology (National Research University), Dolgoprudny, Russia*
[2]*M.V. Lomonosov Moscow State University, Moscow, Russia*
[3]*Institute of Physics CAS, Prague, Czech Republic*
[4]*Faculty of Mathematics and Physics, Charles University, Prague, Czech Republic*
[5]*Nuclear Fuel Cycle Department, Research Centre Rez Ltd., Husinec-Rez, Czech Republic*
[6]*Dresden High Magnetic Field Laboratory (HLD-EMFL), Helmholtz-Zentrum Dresden-Rossendorf (HZDR), Dresden, Germany*
[7]*Technische Universität Dresden, Dresden, Germany*
[8]*Baikov Institute of Metallurgy and Materials Science RAS, Moscow, Russia*
[9]*Peter the Great St. Petersburg Polytechnic University, St. Petersburg, Russia*
[10]*Prokhorov General Physics Institute of RAS, Moscow, Russia*
[11]*Lebedev Physical Institute of the Russian Academy of Sciences, Moscow, Russia*
[12]*Laboratoire National des Champs Magnetiques Intenses (LNCMI-EMFL), CNRS-UJF-UPS-INSA, Toulouse, France*

(Received 26 March 2021; revised 2 June 2021; accepted 10 June 2021; published 9 July 2021)

In this paper, the full magnetization process demonstrated by the series of ferrimagnetic intermetallic compounds (Nd, Ho)$_2$Fe$_{14}$B and Ho$_2$Fe$_{14}$B and their hydrides with the maximum possible hydrogen content (for the given crystal structure type) is studied theoretically and experimentally using megagauss magnetic fields. We observe field-induced phase transitions from the initial ferrimagnetic to the forced-ferromagnetic state in magnetic fields up to 130 T and describe the magnetization process analytically. We find a drastic decrease of the critical transition fields in the hydrogenated compounds. This is due to extremely strong, nearly twofold reduction of the *R*-Fe intersublattice exchange interaction because of the combined substitution and hydrogenation effects. A comparative analysis of the magnetization behavior for the system Ho$_2$Fe$_{17}$-H is also performed.

DOI: 10.1103/PhysRevMaterials.5.074404

I. INTRODUCTION

Improving performance of magnetic materials and extending their applicability toward influential technological areas (e.g., space, robotics, etc.) is an important task fueled both by fundamental and industrial interests [1–3]. To solve this problem, a combined effort of experiment and theory is required. Microstructuring or nanostructuring of magnets together with the addition of various alloying elements and/or light interstitial atoms is known to enhance the functional magnetic properties of the well-known rare earth (*R*) R_2Fe$_{14}$B magnets [4–16]. Modification of the best magnet based on Nd$_2$Fe$_{14}$B by doping is necessary for practical reasons [10,17–19]. For example, thermal stability can be improved by partially substituting neodymium and iron by holmium and cobalt, respectively. This allows us to obtain highly coercive thermostable magnets operating in a wide temperature range.

Modern experimental methods employed in the studies of materials pave the way forward to pursue the task of improving the properties of materials. For instance, for the R_2Fe$_{14}$B compounds with heavy rare earths (ferrimagnets), field-induced ferromagnetism can often be observed only in megagauss (>100 T) magnetic fields accessible at special facilities [20–25]. The ferromagnetic state is usually reached via a series of transitions (i.e., breaking of the antiparallel arrangement of the *R* and Fe magnetic moments). The latter, when analyzed theoretically, provide valuable and accurate information on the internal magnetic parameters of compounds such as crystal electric field and exchange parameters. To this end, analytical methods providing simple and physically understandable description of the physical phenomena need to be developed [26–33].

Despite numerous studies, available information on the intrinsic magnetic properties of the multicomponent intermetallic rare earth compounds of the R_2Fe$_{14}$B type is rather heterogeneous, while a systematic approach is very important from both fundamental and practical points of view [34,35]. We have previously reported [36] a comparative study of the magnetization processes in the system $(R, R')_2$Fe$_{14}$B-H (R = Nd, Ho, Er, and Tm) in high magnetic fields. In this paper, we reveal preparation conditions for the hydrides with the maximum possible hydrogen content $x = 5.5$ at. H/f.u. for the structure 2:14:1 type. We perform a detailed magnetization study of Ho$_2$Fe$_{14}$BH$_x$ and (Nd$_{0.5}$Ho$_{0.5}$)$_2$Fe$_{14}$BH$_x$ ($x = 0$ and 5.5) in magnetic fields up

*Corresponding author: nvkost@gmail.com

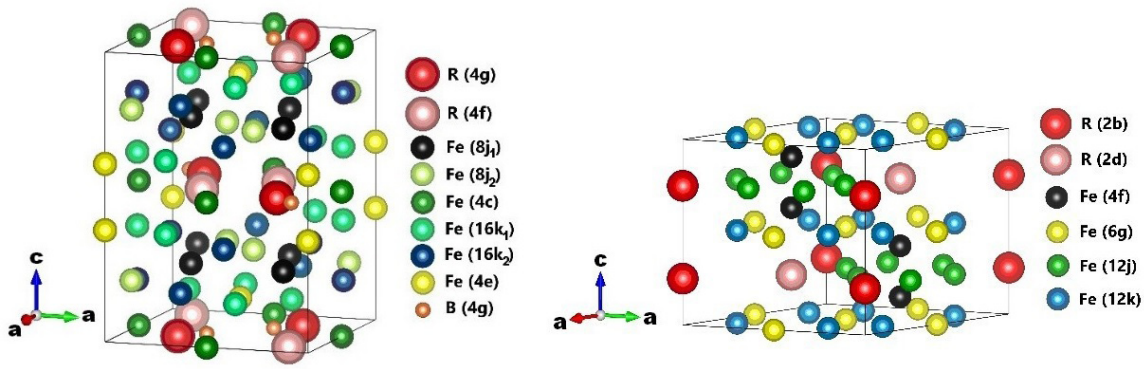

FIG. 1. Crystal structure of the (left) $R_2Fe_{14}B$ (structure is shown schematically, is elongated along an axis twice for the convenience of presentation) and (right) R_2Fe_{17} compounds.

to 130 T. We report a comparative study of the magnetization processes of the 2:14:1 and 2:17-type compounds (Ho_2Fe_{17} and its hydride) using both available literature data [23] and experimental evidence collected in this paper. The approach allows modeling of the magnetization process in the multicomponent $R_2Fe_{14}B$ compounds depending on the type of rare earth, 3*d* metals, light interstitial elements, etc. Theoretical modeling together with experimental data obtained using megagauss magnetic fields permits understanding of the mechanisms of control and variation of internal parameters of the multicomponent compounds on the microscopic level to obtain outstanding of macroscopic properties necessary for practical applications. Using atomistic analytical calculations and megagauss fields, we demonstrate that hydrogenation leads to an extremely strong reduction of the *R*-Fe intersublattice exchange interaction in the $R_2Fe_{14}B$ type of compounds. This is a very attractive tool which can also be applied to other classes of magnetic materials such as, for example, R_2Fe_{17} compounds.

Although the $R_2Fe_{14}B$ compounds have a tetragonal structure [37], but the R_2Fe_{17} compounds (with heavy rare earths) have a hexagonal structure (see Fig. 1), both classes are capable of absorbing up to 5–5.5 at. H/f.u., which favorably distinguishes them from such a class of compounds as $RFe_{11}Ti$ with a tetragonal structure and an absorption capacity of only 1–1.1 at. H/f.u [38].

Due to the large electronegativity difference between the rare earth elements and hydrogen (as observed in many other intermetallic compounds), the insertion of hydrogen is favored in the neighborhood of the rare earth atoms. Hydrogen atoms fill interstitial sites. For the two systems 2:14:1 and 2:17, the filling schemes are slightly different. While in the 2:14:1, pseudotetrahedral sites are filled, in the 2:17 system, first, the octahedral voids are filled up to 3 at. H/f.u., and then tetrahedral voids start to be filled simultaneously with the octahedral ones up to 5 at. H/f.u. The exact filling schemes can be found in Refs. [39–41]. Saturation of the individual interstitial sites is different for various compounds depending on the type of the rare earth (heavy or light), and the stability of the site depends on its size. In connection with the above, a comparative study of magnetization processes for the systems $R_2Fe_{14}B$-H, $(R, R')_2Fe_{14}B$-H, and R_2Fe_{17}-H is relevant and important, especially from a fundamental point of view.

II. EXPERIMENTAL DETAILS

$Ho_2Fe_{14}B$ and $(Nd_{0.5}Ho_{0.5})_2Fe_{14}B$ samples were prepared in a tri-arc furnace on a copper water-cooled bottom under a protective Ar atmosphere. Details of the sample preparation can be found in Refs. [30,35]. Hydrogenation was performed by exposing alloys to high-purity hydrogen obtained by decomposing $LaNi_5H_6$. Before hydrogenation, the sample crushed into submillimeter particles was activated by heating up to 623 K with a heating rate of 0.033 K/s in a dynamic vacuum, then cooled down to 573 K with a rate of 0.017 K/s and kept at this temperature for 12 h [Fig. 2(a)]. The absolute value of pressure in the system before hydrogenation was 0.6 mPa.

Hydrogenation was performed at 573 K under hydrogen pressure of 8 MPa to obtain the maximum hydrogen concentration [Fig. 2(b)]. Hydrogen content was estimated both by a volumetric method (pressure drop in the reaction chamber after the reaction) and by decomposing part of the hydrogenated sample in an evacuated closed system. The following hydrides were obtained: $Ho_2Fe_{14}BH_{5.5}$ and $(Nd_{0.5}Ho_{0.5})_2Fe_{14}BH_{5.5}$. According to Ref. [42], 5.5 hydrogen atoms per formula unit is the maximum possible H content for this type of crystal structure.

Details of synthesis of the parent compound Ho_2Fe_{17} and its hydride $Ho_2Fe_{17}H_{3.4}$ (note that the hydrogen content in this case is lower that the possible maximum content of 5 at. H/f.u. for this structure type [25]) are similar to the other 2:17 compounds production and can be found in Ref. [43]. To test the stability of the hydrides, hydrogen content was analyzed twice upon producing the sample and after a year, during which the sample was stored under normal conditions at room temperature. While $R_2Fe_{14}BH_{5.5}$ hydrides were found to be stable, $R_2Fe_{17}H_X$ with the maximum hydrogen content were not stable. According to Ref. [44], hydrogen concentra-

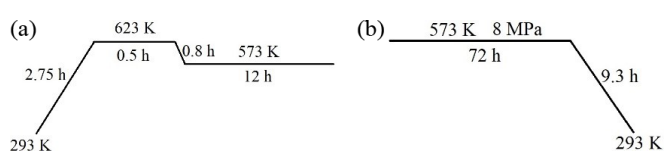

FIG. 2. Schematic of (a) surface activation procedure and (b) hydrogenation of the samples.

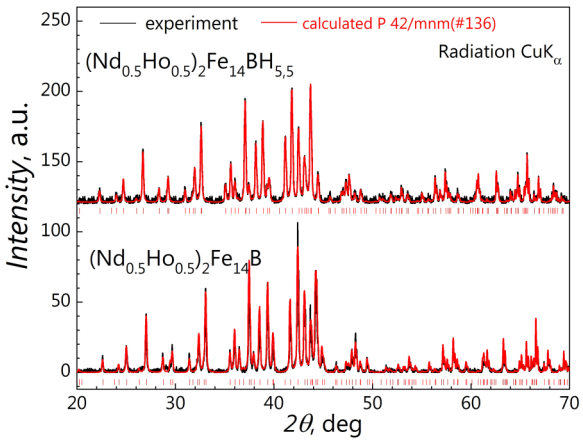

FIG. 3. X-ray diffraction patterns of the $(Nd_{0.5}Ho_{0.5})_2Fe_{14}BH_{5.5}$ and the parent $(Nd_{0.5}Ho_{0.5})_2Fe_{14}B$ alloys at room temperature.

tion decreases from 5.5 to 3–3.4 atoms per formula unit after a year of storage. To be on the safe side, we have chosen a lower hydrogen concentration for the 2:17 compound in this study. Indeed, the $Ho_2Fe_{17}H_{3.4}$ was stable.

The crystal structure of the samples was studied at room temperature by means of x-ray powder diffraction using a Bruker D8 Advance diffractometer (Cu Kα radiation). The crystal structure refinements were based on the Rietveld method, using the program package FULLPROF suite.

Magnetization measurements were performed using high nondestructive magnetic field pulses up to 58 T at the Dresden High Magnetic Field Laboratory [23,45] as well as in megagauss semidestructive pulses up to 135 T at the Laboratoire National des Champs Magnetiques Intenses [46,47]. The magnetization was measured using a compensated pair of coils [23]. For the nondestructive pulses up to 58 T, the pulse duration was 25 ms, and the rise time was 7 ms. In the case of semidestructive experiments, the same magnetic field range was reached in only 1.4 μs corresponding to a 4000 times faster field sweep rate of ~25 ns/T. Magnetization measurements were carried out on free powders for most samples. The particle size of powders did not exceed 50 μm (we performed a two-step grinding to reduce the grain size to 10–50 μm [36]). Experimental results of $M(H)$ were normalized to the static magnetization measurements up to 14 T, which were obtained using a commercial PPMS 14 (Quantum Design, USA) installation.

III. RESULTS AND DISCUSSION

The parent compounds $Ho_2Fe_{14}B$, $(Nd_{0.5}Ho_{0.5})_2Fe_{14}B$, and their hydrides crystallize in the tetragonal crystal structure of the $Nd_2Fe_{14}B$ type ($P4_2/mnm$ tetragonal space group, 68 atoms per unit cell). Iron atoms are in six different crystallographic positions (4*e*, 4*c*, 8*j*1, 8*j*2, 16*k*1, 16*k*2), *R* atoms in two (4*f*, 4*g*), B in one (4*f*; see Fig. 1). Experimentally obtained diffraction spectra of the $(Nd_{0.5}Ho_{0.5})_2Fe_{14}B$ and $(Nd_{0.5}Ho_{0.5})_2Fe_{14}BH_{5.5}$ alloys are shown in Fig. 3.

Good agreement with the calculated $P4_2/mnm$ spectrum is observed, which indicates a high content of the main phase in the alloys. The calculated unit cell parameters are presented in the Table I. The unit cell volume V of the hydrides with the maximum amount of hydrogen exceeds the volume of the parent compounds by ~4%.

TABLE I. Structure parameters for $Ho_2Fe_{14}B$, $(Nd_{0.5}Ho_{0.5})_2Fe_{14}B$, Ho_2Fe_{17} and their hydrides $Ho_2Fe_{14}BH_{5.5}$ $(Nd_{0.5}Ho_{0.5})_2Fe_{14}BH_{5.5}$, $Ho_2Fe_{17}H_{3.4}$

Compounds	a (nm)	c (nm)	c/a	V (nm^3)	$\Delta V/V_0$
$Ho_2Fe_{14}B$	0.8752	1.1991	1.37	0.918	–
$Ho_2Fe_{14}BH_{5.5}$	0.8873	1.2150	1.37	0.956	4.1
$(Nd_{0.5}Ho_{0.5})_2Fe_{14}B$	0.8776	1.2098	1.38	0.932	–
$(Nd_{0.5}Ho_{0.5})_2Fe_{14}BH_{5.5}$	0.8906	1.2227	1.37	0.970	4.1
Ho_2Fe_{17}	0.8449	0.8312	0.98	0.513	–
$Ho_2Fe_{17}H_{3.4}$	0.8531	0.8325	0.98	0.522	1.8

Hydrogenation does not change the type of the crystal lattice but leads to its anisotropic expansion. The unit cell volume V, increases linearly with increasing hydrogen concentration.

Figure 4 shows the magnetization of $Ho_2Fe_{14}B$ and its hydride $Ho_2Fe_{14}BH_{5.5}$ free powder samples measured at 5 K in magnetic fields up to 130 T. The inset in Fig. 2 shows for comparison the magnetization data for Ho_2Fe_{17} (unclamped single-crystal sample, experimental data adapted from Ref. [23]). Figure 5 shows $M(H)$ curves for powder sample Ho_2Fe_{17} and its hydride $Ho_2Fe_{17}H_{3.4}$. Both parent $Ho_2Fe_{14}B$ and Ho_2Fe_{17} compounds demonstrate a well-pronounced kink on the $M(H)$ curves (first critical field H_{c1}) at values close to 40 T (37 T for $Ho_2Fe_{14}B$ and 42.5 T for Ho_2Fe_{17} powder samples) corresponding to the beginning

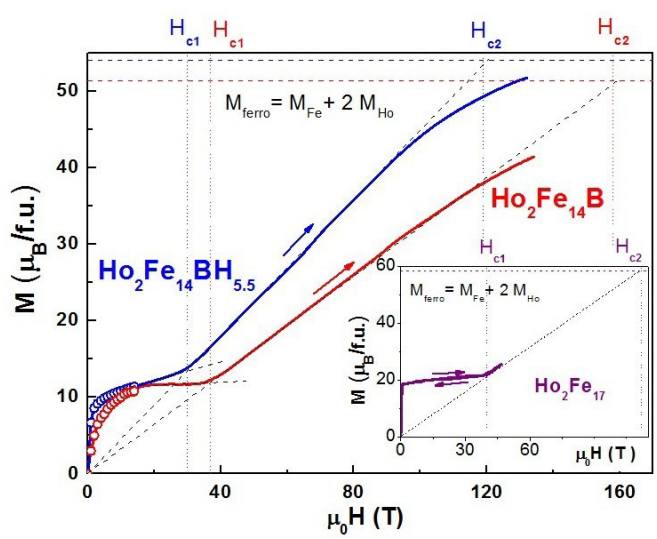

FIG. 4. Experimental magnetization curves of $Ho_2Fe_{14}B$ and its hydrided powder sample $Ho_2Fe_{14}BH_{5.5}$ measured at $T = 5$ K in pulsed fields up to 130 T. By circles, data obtained in static fields up to 14 T are shown. Inset: magnetization data for the Ho_2Fe_{17} unclamped single-crystal sample (experimental data adapted from Ref. [23]) in fields up to 60 T.

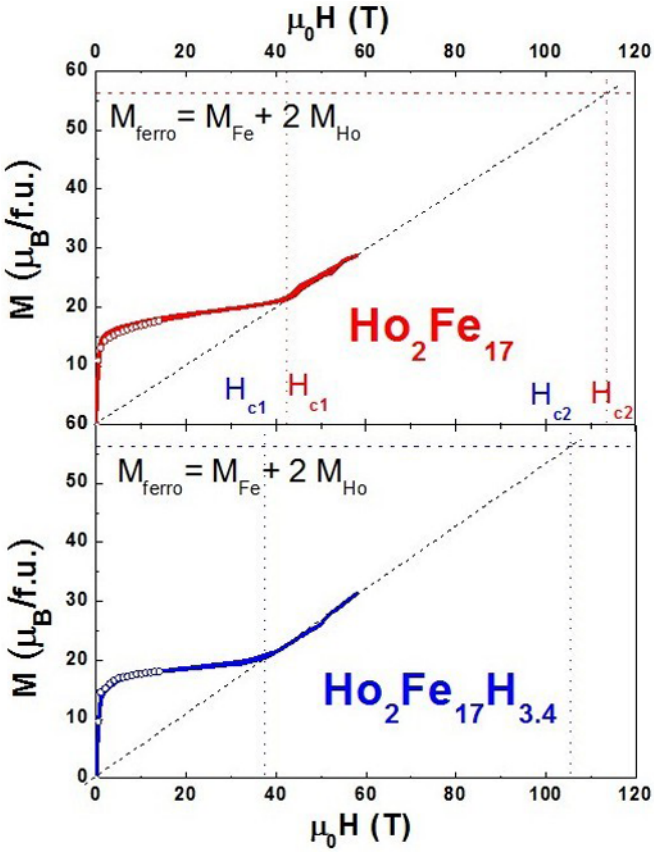

FIG. 5. Experimental magnetization $M(H)$ curves of Ho_2Fe_{17} and its hydrogenated powder sample $Ho_2Fe_{17}H_{3.4}$ measured at $T = 5$ K in pulsed fields up to 60 T. By circles, data obtained in static fields up to 14 T are shown.

of a continuous rotation of magnetic moments of the Ho and Fe sublattices, M_{Ho} and M_{Fe}, respectively. The high-field parts of the $M(H)$ curve can be extrapolated to the origin and to the maximum of magnetization of the ferromagnetic state $M_{ferro} = M_{Fe} + 2M_{Ho}$, at which the magnetic moment rotation is fully completed. The second critical fields H_{c2} in $Ho_2Fe_{14}B$ and Ho_2Fe_{17} corresponding to the end of the spin-reorientation transition to the ferromagnetic state differ strongly for the compounds and amount to 158 T in $Ho_2Fe_{14}B$ and 113.5 T in Ho_2Fe_{17}. Hydrogenation of $Ho_2Fe_{14}B$ to the composition $Ho_2Fe_{14}BH_{5.5}$ results in a decrease of the critical fields H_{c1} and H_{c2} to 30 and 119 T, respectively. At the same time, hydrogenation of Ho_2Fe_{17} to the composition $Ho_2Fe_{17}H_{3.4}$ (see Fig. 5) results in a decrease of the critical fields H_{c1} and H_{c2} to 37.5 and 105.5 T, respectively. This phenomenon, observed for both $Ho_2Fe_{14}BH_x$ and $Ho_2Fe_{17}H_x$ compounds, is undoubtedly directly related to the volume boost by hydrogenation and, hence, to the increase of distances between magneto-active ions.

To analyze all experimental data, we applied the well-proven analytical approach (described in detail in Ref. [42]) to the $R_2Fe_{14}B$-type intermetallic compounds. Recall that

TABLE II. Magnetic parameters (experimental and calculated critical fields H_{c1} and H_{c2}, values of the iron moments M_{Fe}, and the exchange parameter λ) for Ho_2Fe_{17}, $Ho_2Fe_{14}B$, and their hydrides $Ho_2Fe_{17}H_{3.4}$ and $Ho_2Fe_{14}BH_{5.5}$.

Compound	H_{c1} (T) exp./cal.	H_{c2} (T) exp./cal.	$M_{Fe}(\mu_B)$	$\lambda(T/\mu_B)$
Ho_2Fe_{17} [23]	40/40	110/138	36.3	2.45
Ho_2Fe_{17}	42.5/41	113.5/141	36.3	2.5
$Ho_2Fe_{17}H_{3.4}$	37.5/36	105.5/124	36.3	2.2
$Ho_2Fe_{14}B$	37/35	158/158	31.4	3.07
$Ho_2Fe_{14}BH_{5.5}$	30/31	119/119	34	2.2

equations for the critical fields H_{c1} and H_{c2} have the form [27,36,42]

$$H_{c1} = \lambda\,(M_{Fe} - 2M_{Ho}) - \frac{H_a\,2M_{Ho}}{\lambda\,(M_{Fe} - 2M_{Ho})}, \qquad (1)$$
$$H_{c2} = \lambda\,(M_{Fe} + 2M_{Ho}) + \frac{H_a\,2M_{Ho}}{\lambda\,(M_{Fe} + 2M_{Ho})},$$

where λ is the Ho-Fe intersublattice exchange parameter, $H_a = \frac{2K_1}{M_{Fe}}$ is the magnetic anisotropy field, K_1 is magnetic anisotropy constant [5]. Here, the second term describing the anisotropy has been added to make a more accurate critical field estimation [36]. The values of the iron moments M_{Fe} [5,48,49] and the exchange parameter λ are given in Table I. (Note that the magnetic moment of Ho^{3+} ion is $10\,\mu_B$.) Table I also shows experimental and evaluated H_{c1} and H_{c2} values obtained for $Ho_2Fe_{14}B$ and its hydride $Ho_2Fe_{14}BH_{5.5}$, as well as for Ho_2Fe_{17} and $Ho_2Fe_{17}H_{3.4}$ for comparison by analyzing high-field experimental data using the formula in Eq. (1). The results of our estimations of both critical fields listed in Table II agree well with the experimental data for all $Ho_2Fe_{14}BH_x$ compounds. The reason for the different values for the evaluated and experimental data H_{c2} for $Ho_2Fe_{17}H_x$ consists in using magnetic fields only up to 60 T.

Figure 6 shows the magnetization of $(Nd_{0.5}Ho_{0.5})_2Fe_{14}B$ and its hydride powder sample $(Nd_{0.5}Ho_{0.5})_2Fe_{14}BH_{5.5}$ measured at 5 K in semidestructive pulsed magnetic fields up to 130 T. The inset in Fig. 6 demonstrates the experimental difference between the $M(H)$ curves obtained upon increasing and decreasing fields (in semidestructive and nondestructive pulsed magnetic fields [27]) for $(Nd_{0.5}Ho_{0.5})_2Fe_{14}B$. The difference can be due to several reasons (temperature change due to the magnetocaloric effect, state of the sample—magnetized or demagnetized, etc.). We further show the magnetization $M(H)$ data for $(Nd_{0.5}Ho_{0.5})_2Fe_{14}BH_{5.5}$ measured at two different temperatures: 5 and 70 K (see Fig. 7). In addition, the inset in Fig. 7 demonstrates the $M(H)$ curves for the $(Nd_{0.5}Tm_{0.5})_2Fe_{14}BH_{5.5}$ compound since the compounds containing Tm ion require lower external magnetic fields for their complete magnetization. The temperature increase to 70 K leads to a smoother behavior of the $M(H)$ curves, retaining the main features observed at low temperatures for both compounds $(Nd_{0.5}Ho_{0.5})_2Fe_{14}BH_{5.5}$ and $(Nd_{0.5}Tm_{0.5})_2Fe_{14}BH_{5.5}$.

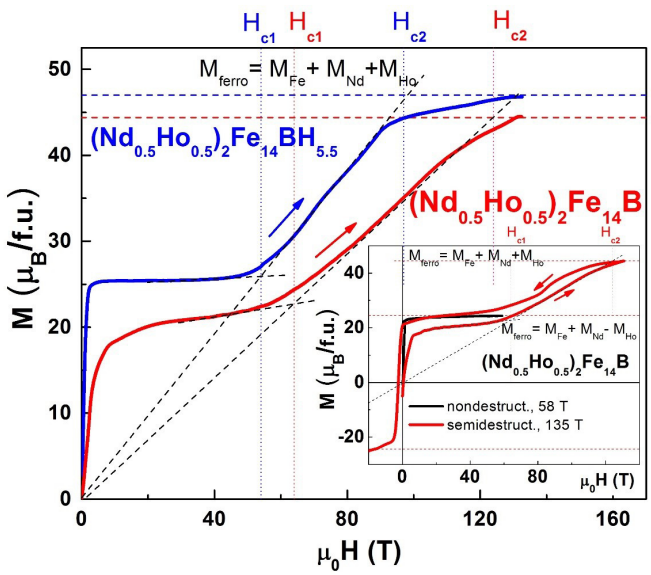

FIG. 6. Experimental magnetization $M(H)$ curves of $(Nd_{0.5}Ho_{0.5})_2Fe_{14}B$ and its hydride $(Nd_{0.5}Ho_{0.5})_2Fe_{14}BH_{5.5}$ powder samples measured at 5 K in semidestructive pulsed magnetic fields. Inset: Experimental magnetization $M(H)$ curves of $(Nd_{0.5}Ho_{0.5})_2Fe_{14}B$ in semidestructive and nondestructive pulsed magnetic fields at 5 K.

We find that, for $(Nd_{0.5}Ho_{0.5})_2Fe_{14}B$ and its hydride $(Nd_{0.5}Ho_{0.5})_2Fe_{14}BH_{5.5}$ in the ferrimagnetic state, the magnetization is close to saturation in magnetic fields 20–40 T (see Figs. 6 and 7). Further increase of magnetic field above the first critical field value H_{c1} [slightly different for $(Nd_{0.5}Ho_{0.5})_2Fe_{14}BH_x$ with $x = 0$ and 5.5 at. H/f.u. and exceeding 40 T] forces the magnetic moments to turn so that we observe a change of slope. The exact experimental values H_{c1} found as the intersection of the saturation magnetic moment in the ferrimagnetic state with linear extrapolations of the $M(H)$

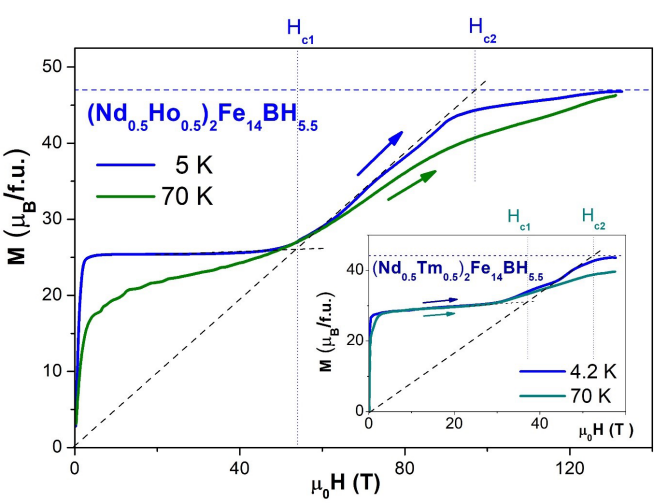

FIG. 7. Experimental magnetization $M(H)$ curves of the $(Nd_{0.5}Ho_{0.5})_2Fe_{14}BH_{5.5}$ powder sample measured at 5 and 70 K. Inset: Experimental magnetization $M(H)$ curves of the $(Nd_{0.5}Tm_{0.5})_2Fe_{14}BH_{5.5}$ powder sample measured at 4.2 and 70 K.

TABLE III. Magnetic parameters (experimental and calculated critical fields H_{c1} and H_{c2}, values of the iron moments M_{Fe}, and the exchange parameter λ) for $(Nd_{0.5}Ho_{0.5})_2Fe_{14}B$ and its hydride $(Nd_{0.5}Ho_{0.5})_2Fe_{14}BH_{5.5}$.

Compound	H_{c1} (T) exp./cal.	H_{c2} (T) exp./cal.	$M_{Fe}(\mu_B)$	$\lambda(T/\mu_B)$
$(Nd_{0.5}Ho_{0.5})_2Fe_{14}B$	64/68	124/124	31.4	3.17
$(Nd_{0.5}Ho_{0.5})_2Fe_{14}BH_{5.5}$	54/55	97/95	34	2.2

curve to zero (see Figs. 6 and 7) are given in Table III for substituted compounds. To determine the critical field H_{c2}, we extrapolated the linear part of our experimental data $M(H)$ to the ferromagnetic saturation (see Figs. 6 and 7) calculated as $M = M_{Fe} + M_{Nd} + M_R$ for $(Nd_{0.5}R_{0.5})_2Fe_{14}B$ (where $R =$ Ho or Tm). The experimental values H_{c2} are also given in Table III.

When half of Ho is replaced by Nd atoms, the saturation magnetization of the $(Nd_{0.5}Ho_{0.5})_2Fe_{14}B$ compound and its hydride $(Nd_{0.5}Ho_{0.5})_2Fe_{14}BH_{5.5}$ in the ferrimagnetic state increases due to the parallel orientation of the magnetic moments of Nd and Fe sublattices. On the contrary, the saturation magnetization in the ferromagnetic state decreases due to a smaller magnetic moment of Nd^{3+} than Ho^{3+} (3 and 10 μ_B, respectively). It should also be noted that the magnetization in the ferrimagnetic phase of the hydrogen-doped compound is higher than that of the hydrogen-free sample. This is due to the increased magnetic moment of the iron sublattice after hydrogenation as the result of the unit cell volume expansion [5] (see Tables II and III).

For the $(Nd_{0.5}Ho_{0.5})_2Fe_{14}BH_x$ ($x = 0$ and 5.5 at. H/f.u.) compounds with two different rare earth ions, the critical fields H_{c1} and H_{c2} are equal to [36]

$$H_{c1} = \lambda_{Ho}(M_{Fe} - 2M_{Ho}\xi_1) - \frac{2M_{Ho}H_a\xi_1^2}{(M_{Fe} - 2M_{Ho}\xi_1)}, \quad (2)$$

$$H_{c2} = \lambda_{Ho}(M_{Fe} + 2M_{Ho}\xi_2) + \frac{2M_{Ho}H_a\xi_2^2}{(M_{Fe} + 2M_{Ho}\xi_2)},$$

$$\xi_i(H_{ci}) = \frac{1}{1 + \lambda_{Nd}\chi_{Nd}(H_{ci})};$$

$$\chi_{Nd}(H_{ci}) = \frac{2M_{Nd}}{\lambda_{Nd}M_{Fe} + H_{ci}}; \qquad i = 1, 2,$$

where λ_{Nd} and χ_{Nd} are the exchange parameter and susceptibility of the Nd sublattice, respectively. According to our estimations, $\xi_i \approx 0.9$ [42]. The formulae in Eq. (2) with anisotropic correction are universal and could be used for various types of compounds containing rare earth elements. Calculated H_{c1} and H_{c2} values obtained for $(Nd_{0.5}Ho_{0.5})_2Fe_{14}B$ and $(Nd_{0.5}Ho_{0.5})_2Fe_{14}BH_{5.5}$ by analyzing high-field experimental data using the formula in Eq. (2) and the values of the iron moments and the exchange parameter λ are given in Table III. Despite the fact that the anisotropy values for powder samples are not exactly known, we observe a very good agreement between the experimental and calculated values of critical fields H_{c1} and H_{c2} (see Table III). The accuracy of analytical determination of the values of both critical fields reaches several Tesla. Nevertheless, they provide important

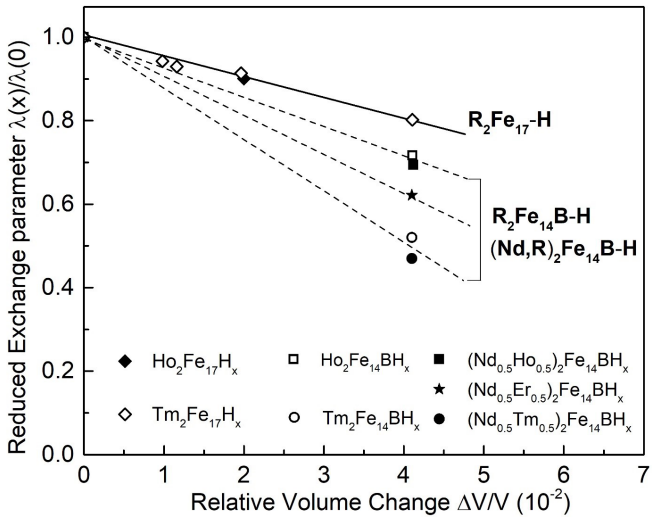

FIG. 8. Reduced exchange parameters λ for $R_2Fe_{17}H_x$ (R = Ho, Tm [54]), $R_2Fe_{14}BH_x$ and (Nd, R)$_2$Fe$_{14}$BH$_x$ (R = Ho, Er [36], and Tm [36]) as a function of the relative volume change $\Delta V/V$.

information on the magnitude of magnetic fields required to reach the ferromagnetic state and allow us to plan high-field magnetization experiments for studying similar compounds.

An extremely important result of our research is the observation of a drastic influence of hydrogenation on the critical fields regardless of the rare earth element. For $Ho_2Fe_{14}BH_x$ and $(Nd_{0.5}Ho_{0.5})_2Fe_{14}BH_x$ compounds (for x from 0 to 5.5), H_{c1} and H_{c2} decrease by ∼16–19% and 22–25%, respectively. This is due to the weakening of the intersublattice exchange interactions by ∼30% (see the λ values in Tables II and III) by doping the compounds with the maximum possible amount of hydrogen. At the same time, our calculations show that the difference in the parameter λ for the binary compound Ho_2Fe_{17} and ternary compound $Ho_2Fe_{14}B$ is ∼20%, which is fully consistent with literature [50–53] and confirms the correctness of our approach when analyzing experimental data obtained using megagauss magnetic fields.

Summarizing the data obtained, we also plot the reduced exchange parameters (shown along the y axis in Fig. 8) λ for $R_2Fe_{17}H_x$ (R = Ho, Tm [54]), $R_2Fe_{14}BH_x$, and (Nd, R)$_2$Fe$_{14}$BH$_x$ (R = Ho, Er [36], and Tm [36]) as a function of the relative volume change $\Delta V/V$ (see Fig. 8).

While the $\lambda(x)/\lambda(0)$ vs $\Delta V/V$ dependence is linear for the R_2Fe_{17}-H system, this is not the case for $R_2Fe_{14}B$-H. At the end of the series of rare earth ions (moving from holmium to thulium), a noticeable decrease in the value of the exchange parameter occurs. Lanthanide contraction and magnetoelastic effects affect the intersublattice exchange interactions to a much larger extent for the $R_2Fe_{14}B$-H system than the R_2Fe_{17}-H due to the higher percentage ratio of R/Fe.

IV. SUMMARY

To summarize, in this paper, we simultaneously involved three powerful tools for tuning the magnetic properties of the $R_2Fe_{14}B$-type compounds. Targeted modification of the ferrimagnetic intermetallics by substitutional and interstitial atoms led to an increase in the magnetization of the compounds. The use of megagauss magnetic fields made it possible to observe the full magnetization process in materials, which is especially important for fundamental research. We determined values of both critical fields and estimated parameter λ of the intersublattice R-Fe exchange interaction for all studied $R_2Fe_{14}B$-type compounds, including compositions of practical importance. We showed that hydrogen influences dramatically the strength of the R-Fe exchange interaction (it is decreasing by 30%) and thus can be used as a control tool over magnetic properties. The reduced values of critical fields of the transitions H_{c1} and H_{c2} after hydrogenation allowed us to observe the forced-ferromagnetic state for $(Nd_{0.5}R_{0.5})_2Fe_{14}BH_x$ compositions with the maximum possible hydrogen content (x = 5.5 at. H/f.u.) in much lower fields than the hydrogen-free materials.

ACKNOWLEDGMENTS

This work was performed with financial support of the Russian Science Foundation (Project No. 18-13-00135). We acknowledge the support from LNCMI Toulouse and the HLD at HZDR, members of the European Magnetic Field Laboratory (EMFL). The work of E.A.T.-Ch. is supported by the project Nanomaterials Centre for Advanced Applications, Project No. CZ.02.1.01/0.0/0.0/15_003/0000485, financed by the European Regional Development Fund. The work of A.K.Z. is supported by the Russian Foundation for Basic Research, Project No. 18-02-00994. This paper was supported by Project No. 19-00925S of the Czech Science Foundation and by Materials Growth & Measurement Laboratory within the Program of Czech Research Infrastructures (Project No. LM2018096).

[1] J. M. D. Coey, Hard magnetic materials: a perspective, IEEE Trans. Mag. **47**, 4671 (2011).

[2] J. M. D. Coey, Perspective and prospects for rare earth permanent magnets, Engineering **6**, 119 (2020).

[3] O. Gutfleisch, M. A. Willard, E. Brück, C. H. Chen, S. G. Sankar, and J. Ping Liu, Magnetic materials and devices for the 21st century: stronger, lighter, and more energy efficient, Adv. Mater. **23**, 821 (2011).

[4] H. Sepehri-Amin, S. Hirosawa, and K. Hono, Chapter 4—advances in Nd-Fe-B based permanent magnets, Handb. Magn. Mater. **27**, 269 (2018).

[5] J. F. Herbst, $R_2Fe_{14}B$ materials: intrinsic properties and technological aspects, Rev. Mod. Phys. **63**, 819 (1991).

[6] H.-S. Li and J. M. D. Coey, Chapter 3—magnetic properties of ternary rare-earth transition-metal compounds, Handb. Magn. Mater. **28**, 87 (2019).

[7] A. M. Gabay, M. Marinescu, W. F. Li, J. F. Liu, and G. C. Hadjipanayis, Dysprosium-saving improvement of coercivity in Nd-Fe-B sintered magnets by Dy_2S_3 additions, J. Appl. Phys. **109**, 083916 (2011).

[8] W.-Q. Liu, C. Chang, M. Yue, J.-S. Yang, D.-T. Zhang, J.-X. Zhang, and Y.-Q. Liu, Coercivity, microstructure, and thermal

stability of sintered Nd-Fe-B magnets by grain boundary diffusion with TbH_3 nanoparticles, Rare Met. **36**, 718 (2017).

[9] I. S. Tereshina, I. A. Pelevin, E. A. Tereshina, G. S. Burkhanov, K. Rogacki, M. Miller, N. V. Kudrevatykh, P. E. Markin, A. S. Volegov, R. M. Grechishkin, S. V. Dobatkin, and L. Schultz, Magnetic hysteresis properties of nanocrystalline (Nd,Ho)-(Fe,Co)-B alloy after melt spinning, severe plastic deformation and subsequent heat treatment, J. Alloys. Compd. **681**, 555 (2016).

[10] T.-H. Kim, S.-R. Lee, H.-J. Kim, M.-W. Lee, and T.-S. Jang, Magnetic and microstructural modification of the Nd-Fe-B sintered magnet by mixed DyF_3/DyH_x powder doping, J. Appl. Phys. **115**, 17A763 (2014).

[11] T. Horikawa, M. Yamazaki, C. Mishima, M. Matsuura, and S. Sugimoto, Magnetic anisotropy and crystallographic alignment in Fe and NdH_2 during d-HDDR process of Nd-Fe-B-Ga-Nb powders, AIP Adv. **9**, 035244 (2019).

[12] R. S. Sheridan, I. R. Harris, and A. Walton, The development of microstructure during hydrogenation-disproportionation-desorption-recombination treatment of sintered neodymium-iron-boron-type magnets, J. Magn. Magn. Mater. **401**, 455 (2016).

[13] I. Poenaru, A. Lixandru, K. Güth, A. Malfliet, S. Yoon, I. Škulj, and O. Gutfleisch, HDDR treatment of Ce-substituted $Nd_2Fe_{14}B$-based permanent magnet alloys—phase structure evolution, intergranular processes and magnetic property development, J. Alloys. Compd. **814**, 152215 (2020).

[14] I. Titov, D. Honecker, D. Mettus, A. Feoktystov, J. Kohlbrecher, P. Strunz, and A. Michels, Anisometric mesoscale nuclear and magnetic texture in sintered Nd-Fe-B magnets, Phys. Rev. Materials **4**, 054419 (2020).

[15] S. Kobayashi, A. Martín-Cid, K. Toyoki, H. Okazaki, S. Kawaguchi, S. Hirosawa, and T. Nakamura, Effects of texture on lattice constants of $Nd_2Fe_{14}B$ and their relationship with internal stress in Nd-Fe-B permanent magnets, Phys. Rev. Materials **4**, 094405 (2020).

[16] H. İ. Sözen, S. Ener, F. Maccari, K. P. Skokov, O. Gutfleisch, F. Körmann, J. Neugebauer, and T. Hickel, *Ab initio* phase stabilities of Ce-based hard magnetic materials and comparison with experimental phase diagrams, Phys. Rev. Materials **3**, 084407 (2019).

[17] E. P. Furlani, *Permanent Magnet and Electromechanical Devices: Materials, Analysis, and Applications* (Academic Press, San Diego, 2001).

[18] J. Chaboy, C. Piquer, N. Plugaru, F. Bartolomé, M. A. Laguna-Marco, and F. Plazaola, ^{57}Fe Mössbauer and x-ray magnetic circular dichroism study of magnetic compensation of the rare-earth sublattice in $Nd_{2-x}Ho_xFe_{14}B$ compounds, Phys. Rev. B **76**, 134408 (2007).

[19] I. S. Tereshina, N. V. Kudrevatykh, L. A. Ivanov, G. A. Politova, E. A. Tereshina, D. Gorbunov, M. Doerr, and K. Rogacki, Magnetic properties of the nanocrystalline Nd-Ho-Fe-Co-B alloy at low temperatures: the influence of time and annealing, J. Mat. Eng. Perf. **26**, 4676 (2017).

[20] H. Kato, D. W. Lim, M. Yamada, Y. Nakagawa, H. Aruga Katori, and T. Goto, Field-induced phase transitions in ferrimagnetic $R_2Fe_{14}B$ in ultra-high magnetic fields, Physica B **211**, 105 (1995).

[21] I. S. Tereshina, L. A. Ivanov, E. A. Tereshina-Chitrova, D. I. Gorbunov, M. A. Paukov, L. Havela, H. Drulis, S. A. Granovsky, M. Doerr, V. S. Gaviko, and A. V. Andreev, Tailoring the ferrimagnetic-to-ferromagnetic transition field by interstitial and substitutional atoms in the *R*-Fe compounds, Intermetallics **112**, 106546 (2019).

[22] N. V. Kostyuchenko, A. K. Zvezdin, E. A. Tereshina, Y. Skourski, M. Doerr, H. Drulis, I. A. Pelevin, and I. S. Tereshina, High-field magnetic behavior and forced-ferromagnetic state in an $ErFe_{11}TiH$ single crystal, Phys. Rev. B **92**, 104423 (2015).

[23] Y. Skourski, M. D. Kuz'min, K. P. Skokov, A. V. Andreev, and J. Wosnitza, High-field magnetization of Ho_2Fe_{17}, Phys. Rev. B **83**, 214420 (2011).

[24] I. S. Tereshina, M. Doerr, Y. Skourski, E. A. Tereshina, K. Watanabe, I. V. Telegina, and H. Drulis, High-field magnetization study of $R_2Fe_{17}H_3$ (R = Tb, Dy, Ho and Er) single-crystalline hydrides, IEEE Trans. Mag. **47**, 3617 (2011).

[25] G. S. Burkhanov, I. S. Tereshina, M. A. Paukov, I. A. Pelevin, S. A. Nikitin, R. Bezdushnyi, R. Damianova, E. A. Tereshina, and H. Drulis, Magnetic phase diagrams of the Tm_2Fe_{17}-H system, Dokl. Phys. Chem. **469**, 102 (2006).

[26] Y. Tatetsu, S. Tsuneyuki, and Y. Gohda, First-Principles Study of the Role of Cu in Improving the Coercivity of Nd-Fe-B Permanent Magnets, Phys. Rev. Appl. **6**, 064029 (2016).

[27] A. K. Zvezdin, Magnetic phase transitions: field-induced (order-to-order), in *Encyclopedia of Materials: Science and Technology*, edited by K. H. J. Buschow, R. W. Cahn, M. C. Flemings, B. Ilschner, E. J. Kramer, S. Mahajan, and P. Veyssière (Elsevier Science, Oxford, 2001), pp. 4841–4847.

[28] S. C. Westmoreland, R. F. L. Evans, G. Hrkac, T. Schrefl, G. T. Zimanyi, M. Winklhofer, N. Sakuma, M. Yano, A. Kato, T. Shoji, A. Manabe, M. Ito, and R. W. Chantrell, Multiscale model approaches to the design of advanced permanent magnets, Scripta Mater. **148**, 56 (2018).

[29] C. Benabderrahmane, P. Berteaud, M. Valléau, C. Kitegi, K. Tavakoli, N. Béchu, A. Mary, J. M. Filhol, and M. E. Couprie, $Nd_2Fe_{14}B$ and $Pr_2Fe_{14}B$ magnets characterization and modelling for cryogenic permanent magnet undulator applications, Nucl. Instrum. Meth. Phys. Res. **669**, 1 (2012).

[30] N. V. Kostyuchenko, I. S. Tereshina, D. I. Gorbunov, E. A. Tereshina-Chitrova, A. V. Andreev, M. Doerr, G. A. Politova, and A. K. Zvezdin, Features of magnetization behavior in the rare-earth intermetallic compound $(Nd_{0.5}Ho_{0.5})_2Fe_{14}B$, Intermetallics **98**, 139 (2018).

[31] M. Ito, M. Yano, N. Dempsey, and D. Givord, Calculations of the magnetic properties of $R_2M_{14}B$ intermetallic compounds (R = rare earth, M = Fe, Co), J. Magn. Magn. Mat. **400**, 379 (2016).

[32] K. Kawasaki, T. Yanai, M. Nakano, and H. Fukunaga, Computer simulation of enhancement of coerciviy in Nd-Fe-B/(Nd,Dy)-Fe-B composite magnets, J. Magnetics **16**, 145 (2011).

[33] Q. Gong, M. Yi, and B.-X. Xu, Multiscale simulations toward calculating coercivity of Nd-Fe-B permanent magnets at high temperatures, Phys. Rev. Materials **3**, 084406 (2019).

[34] J. Chaboy, N. Plugaru, J. Bartolome, and G. Subias, Enhancement of anisotropy in $Nd_2Fe_{14}B$ driven by Eu substitution, Phys. Rev. B **67**, 014415 (2003).

[35] G. A. Politova, I. S. Tereshina, D. I. Gorbunov, M. A. Paukov, A. V. Andreev, R. M. Grechishkin, and K. Rogacki, Magnetic and magnetocaloric properties of single crystal $(Nd_{0.5}Pr_{0.5})_2Fe_{14}B$, J. Alloys. Compd. **751**, 283 (2018).

[36] N. V. Kostyuchenko, I. S. Tereshina, A. V. Andreev, M. Doerr, E. A. Tereshina-Chitrova, M. A. Paukov, D. I. Gorbunov, G. A. Politova, A. P. Pyatakov, A. Miyata, O. Drachenko, A. K. Zvezdin, and O. Portugall, Investigation of the field-induced phase transitions in the $(R, R')_2Fe_{14}B$ rare-earth intermetallics in ultra-high magnetic fields, IEEE Trans. Magn. **57**, 2101105 (2021).

[37] J. F. Herbst, J. J. Croat, and W. B. Yelon, Structural and magnetic properties of $Nd_2Fe_{14}B$ (invited), J. Appl. Phys. **57**, 4086 (1985).

[38] I. S. Tereshina, N. V. Kostyuchenko, E. A. Tereshina-Chitrova, Y. Skourski, M. Doerr, I. A. Pelevin, A. K. Zvezdin, M. Paukov, L. Havela, and H. Drulis, $ThMn_{12}$-type phases for magnets with low rare-earth content: crystal-field analysis of the full magnetization process, Sci. Rep. **8**, 3595 (2018).

[39] S. Obbade, S. Miraglia, P. Wolfers, J. L. Soubeyroux, D. Fruchart, F. Lera, C. Rillo, B. Malaman, and G. le Caer, Structural and magnetic study of $Ho_2Fe_{14}BH_x$ ($x = 0$–3.1), J. Less Common Met. **171**, 71 (1991).

[40] O. Isnard, W. B. Yelon, S. Miraglia, and D. Fruchart, Neutron-diffraction study of the insertion scheme of hydrogen in $Nd_2Fe_{14}B$, J. Appl. Phys. **78**, 1892 (1995).

[41] O. Isnard, S. Miraglia, J. L. Soubeyroux, D. Fruchart, and P. l'Héritier, A structural analysis and some magnetic properties of the $R_2Fe_{17}H_x$ series, J. Magn. Magn. Mater. **137**, 151 (1994).

[42] I. S. Tereshina, A. P. Pyatakov, E. A. Tereshina-Chitrova, D. I. Gorbunov, Y. Skourski, J. M. Law, M. A. Paukov, L. Havela, M. Doerr, A. K. Zvezdin, and A. V. Andreev, Probing the exchange coupling in the complex modified Ho-Fe-B compounds by high-field magnetization measurements, AIP Adv. **8**, 125223 (2018).

[43] S. V. Veselova, M. A. Paukov, I. S. Tereshina, V. N. Verbetsky, K. V. Zakharov, D. I. Gorbunov, and A. N. Vasil'ev, Synthesis, structure and magnetic properties of $Sm_{1.2}Ho_{0.8}Fe_{17}H_x$ ($x = 0; 4.4$), J. Rare Earths, doi: 10.1016/j.jre.2020.08.010.

[44] M. A. Paukov, L. A. Ivanov, D. I. Gorbunov, and I. S. Tereshina, Magnetic and magnetothermal properties of hydrogenated materials based on rare earths and iron, IEEE Magn. Lett. **10**, 2508705 (2019).

[45] S. Zherlitsyn, B. Wustmann, T. Herrmannsdorfer, and J. Wosnitza, Status of the pulsed-magnet-development program at the Dresden high magnetic field laboratory, IEEE Trans. Appl. Supercond. **22**, 4300603 (2012).

[46] O. Portugall, N. Puhlmann, H. U. Müller, M. Barczewski, I. Stolpe, and M. von Ortenberg, Megagauss magnetic field generation in single-turn coils: new frontiers for scientific experiments, J. Phys. D: Appl. Phys. **32**, 2354 (1999).

[47] S. Takeyama, R. Sakakura, Y. H. Matsuda, A. Miyata, and M. Tokunaga, Precise magnetization measurements by parallel self-compensated induction coils in a vertical single-turn coil up to 103 T, J. Phys. Soc. Jpn. **81**, 014702 (2011).

[48] E. A. Tereshina and A. V. Andreev, Magnetization and specific heat study of metamagnetism in Lu_2Fe_{17}-based intermetallic compounds, Intermetallics **18**, 1205 (2010).

[49] S. A. Nikitin, I. S. Tereshina, N. Y. Pankratov, E. A. Tereshina, Y. V. Skourski, K. P. Skokov, and Y. G. Pastushenkov, Magnetic anisotropy and magnetostriction in a Lu_2Fe_{17} intermetallic single crystal, Phys. Solid State **43**, 1720 (2001).

[50] R. Verhoef, P. H. Quang, J. J. M. Franse, and R. J. Radwański, The strength of the R-T exchange coupling in $R_2Fe_{14}B$ compounds, J. Magn. Magn. Mater. **83**, 139 (1990).

[51] R. J. Radwański and J. J. M. Franse, Rare earth magnetocrystalline anisotropy in $R_2Fe_{14}B$ compounds—high-field magnetization process, J. Magn. Magn. Mater. **74**, 43 (1988).

[52] S. Sinnema, Magnetic interactions in R_2T_{17} and $R_2T_{14}B$ intermetallic compounds, Ph.D. thesis, Natuurkundig Laboratorium, University of Amsterdam, Netherlands, 1988.

[53] W. Kyoko and M. Motokawa, eds., *Materials Science in Static High Magnetic Fields* (Springer, Berlin and Heidelberg, 2012).

[54] E. A. Tereshina, M. D. Kuz'min, Y. Skourski, M. Doerr, W. Iwasieczko, J. Wosnitza, and I. S. Tereshina, Forced-ferromagnetic state in a $Tm_2Fe_{17}H_5$ single crystal, J. Phys. Condens. Matter **29**, 24LT01 (2017).